Catalytic Properties of Platinum Nanoparticles Obtained in a Single Step Simultaneous Reduction of Pt(IV) Ions and Graphene Oxide

Marek Wojnicki[1]*, Magdalena Luty-Błocho[1], Krzysztof Mech[2], Justyna Grzonka[3], Krzysztof Fitzner[1] and Krzysztof J. Kurzydłowski[3]

[1]*Faculty of Non-Ferrous Metals, Department of Physical Chemistry and Metallurgy of Non-Ferrous Metals, AGH University of Science and Technology, al. A. Mickiewicza 30, 30-059, Krakow, Poland*
[2]*AGH University of Science and Technology, Academic Centre for Materials and Nanotechnology, al. A. Mickiewicza 30, 30-059, Krakow, Poland*
[3]*Warsaw University of Technology, Faculty of Materials Science and Engineering, ul. Wołoska, 141, 02-507, Warsaw, Poland*

Received: 08 September 2014; accepted: 24 November 2014

A composite material consisting of metallic platinum nanoparticles and reduced graphene oxide was successfully obtained in microflow reactor. Moreover, subnanometric platinum particles were observed. Reduced graphene oxide plays an important role as a stabilizing agent for platinum nanoparticles. Reduced graphene oxide coverage and platinum particle size as well as size distribution depend mainly on initial concentration of platinum(IV) ions. High level of reduced graphene oxide coverage by platinum nanoparticles (PtNPs) was obtained and is equal to 71%. This in turn effects significantly the mass ratio of reduced graphene oxide to PtNPs which is equal to 49% (w/w). Fourier transform infrared (FT-IR) and X-ray photoelectron spectroscopy (XPS) analysis of the obtained materials were performed. Also, catalytic properties of the obtained composite material consisting of PtNPs at reduced graphene oxide surface, towards electrochemical glucose oxidation, were investigated. It was found that the studied materials exhibit high catalytic activity for glucose electro-oxidation process.

Keywords: platinum nanoparticles, graphene oxide, microreactor, microflow reactor, deposition, DMAB, glucose electro-oxidation

1. Introduction

Graphene is one of the most interesting materials found during the last decade. Since the last few years, a significant number of papers [1] and books [2] have been published and dedicated to graphene and graphene oxide. Graphene as well as graphene oxide can find potential applications in electronic and nanoelectronic systems. Preparation of graphene oxide is less expensive than graphene. It is a reason why most works are focused on graphene oxide. Thanks to high thermal and electrical conductivity, graphene offers more than commonly applied materials. However, there are still some problems with the large scale graphene preparation. For this reason, the common route is to synthesize graphene oxide using one of the well-known methods and then reduce it to obtain graphene [1b, 3].

Graphene is probably one of the most chemically resistant materials. It does not dissolve in mineral acids and organic solvents. From this point of view, graphene seems to be excellent substrate for catalytic application. On the other hand, this feature seems to be also a disadvantage because of a problem with the catalyst deposition on graphene surface using hydrometallurgical methods since the graphene exhibit hydrophobic nature [4]. To make it possible, graphene oxide is often used as a precursor. After chemical modification of graphene oxide (GO), gold [5], silver [6], platinum [7], palladium [7b], and other metals can be deposited on its surface.

It is well known that nanoparticles of platinum and its alloys exhibit great catalytic properties [8], among them are electrocatalytic oxidation of glucose (Pt–Pd alloy [9], Au–Pt nanocomposite [10], and PtRu–C [11]) and methanol electro-oxidation [10b, 12]. Also, platinum-based materials are widely used in fuel cells [7a]. Unsupported nanoparticles are rarely used in catalysis due to the problem with catalyst separation from remaining reagents. From this reason, platinum nanoparticles are commonly deposited on different carriers, with one of the most popular materials, being carbon-based structures such as carbon fibers [13], activated carbon [14], graphene [7a], carbon nanotubes [15], etc.

To synthesize particles of graphene oxide or graphene decorated with precious metal nanoparticles, several steps are commonly required. The first one is related to graphene oxide synthesis and chemical modification of GO surface, and the last one to nanoparticles synthesis and deposition on GO surface. Each step needs specific chemical reagents and takes a considerable time (even 24 h) [12c]. In this context, we would like to demonstrate here a single step synthesis of platinum nanoparticles and their deposition on graphene oxide sheets in the seconds scale time. For this purpose, microreactor (also commonly called microflow reactor) was used. The greatest advance of application of microflow reactors is the opportunity to decrease the amount of wastes generated during the experiments as well as in the future in the industrial scale. Also, it should be pointed out that microflow reactors possess significant surface to volume ratio. This in turn allows for rapid increase or decrease of temperature of reagent especially in the case of endothermic or exothermic reactions, respectively [16]. Also, scale-up of production can be easily achieved, by connecting new reactors in parallel. Moreover, reducing several steps into one is possible using flow chemistry, which may result in cost reduction in production.

Microflow reactors have been previously used in metal nanoparticles synthesis [17]; however, there are only a few papers where microflow systems have been used for composite materials synthesis [5c, 18]. Analyzing recent development of the synthesis of the noble metal nanoparticles in micro and milifluidic devices as well as their catalytic application, Shahbazali et al. pointed out that the reaction performance can be remarkably improved by the mineralization of the reaction time [8].

2. Results and Discussion

2.1. Influence of Platinum(IV) Initial Concentration on Particle Size and Size Distribution. The influence of initial concentration of platinum(IV) complex ions on particle size and size distribution has been investigated by applying constant

* Author for correspondence: marekw@agh.edu.pl

DOI: 10.1556/JFC-D-14-00032

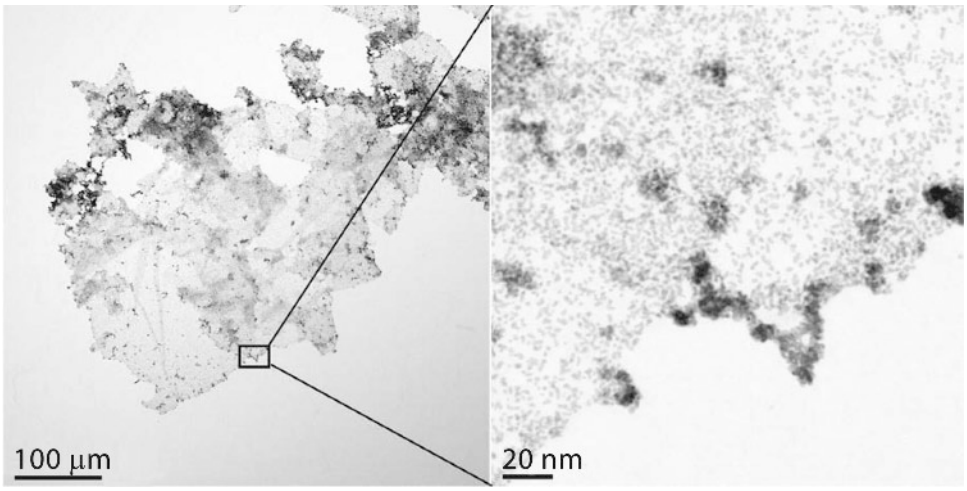

Figure 1. HRTEM image of platinum nanoparticles deposited on graphene oxide sheets (experimental conditions: $C_{0,Pt(IV)}=8.3\times10^{-5}$ M, $C_{0,GO}=1\times10^{-1}$ g/L, $C_{0,DMAB}=1\times10^{-2}$ M, pH=13)

initial concentrations of reductant (1×10^{-2} M) and graphene oxide (1×10^{-1} g/L). Constant flow rate of each reagent was equal to 1 mL/min. It was observed that for platinum(IV) complex ions with initial concentration in the range from 3.3×10^{-5} to 8.3×10^{-5} M, all nanoparticles were adsorbed on graphene oxide as shown in Figure 1. For the sample obtained at Pt(IV) initial concentration of 2.5×10^{-4} M, a significant number of platinum nanoparticles did not adsorb onto graphene oxide, remaining in the solution as colloidal particles (Figure 2).

To confirm the conclusions drawn from high-resolution transmission electron microscopy (HRTEM) images of the adsorption NPs (Figure 1), the following experiment was performed. About 5 mL of the suspension containing platinum nanoparticles adsorbed on graphene oxide was filtered using syringe filter (200 nm pore size, membrane material — refracted cellulose). Then, the obtained filtrate was mixed in the proportion 1:1 per volume with freshly prepared aqueous regia to dissolve platinum nanoparticles left in the solution. In the next step, the obtained solution was analyzed using atomic absorption spectroscopy (Thermo Scientific, Solar). In the analyzed sample, the platinum level was below detection limits for this photometer (in our case, ~1 ppm). This in turn can be a final proof that more than 99% of all nanoparticles are adsorbed on the surface of graphene oxide.

To perform X-ray photoelectron spectroscopy (XPS) analysis of the obtained material, a sample was prepared by sequential drop-casting and evaporation of the solvent from the suspension in vacuum drier. Then, the XPS spectra were recorded. The obtained results are shown in Figure 3. The spectra collected at Pt4f region can be fitted with two doublet structures where $Pt4f_{7/2}$ peaks are centered at binding energies of 72.5 eV and 74.2 eV. They are attributed to Pt^{2+} [19] and Pt^{4+} states [20], respectively. The estimated fraction of Pt^{2+} is equal to 91 at.%.

The Pt^{2+} can be related to PtO or $Pt(OH)_2$ species. However, it cannot be excluded that this peak is related to platinum nanoparticles (PtNPs), and the shift of binding energy is caused by strong electrophilic substrate [21]. In the case of Pt^{4+}, two types of structure can be proposed: the first one is PtO_2, and the second one is $Pt(OH)_4$.

To explain this uncertainty, further analysis was performed. Fast Fourier transform (FFT) of registered HRTEM picture (Figure 4A) revealed that interplanar distance determined from FFT analysis (Figure 4B) corresponds to Pt(-111) and Pt(020) planes and equals to 0.23 and 0.2, respectively.

Figure **5** shows the size distribution diagrams of particles bonded to graphene oxide surface ("A–D"), as well as those not bonded to it ("E").

The maintenance of a narrow distribution of the nanoparticles can be obtained by reducing the mean diffusion paths of reactants in micromixer (see Figure 12). In conventional micromixer, the paths of the diffusion are equal to the diameter of

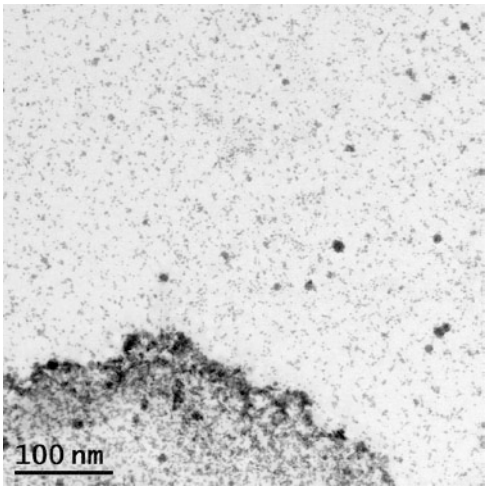

Figure 2. HRTEM image of platinum nanoparticles loaded graphene oxide sheets and in its surroundings ($C_{0,Pt(IV)}=2.5\times10^{-4}$ M, $C_{0,GO}=3\times10^{-2}$ g/L, $C_{0,DMAB}=3\times10^{-3}$ M, pH=13)

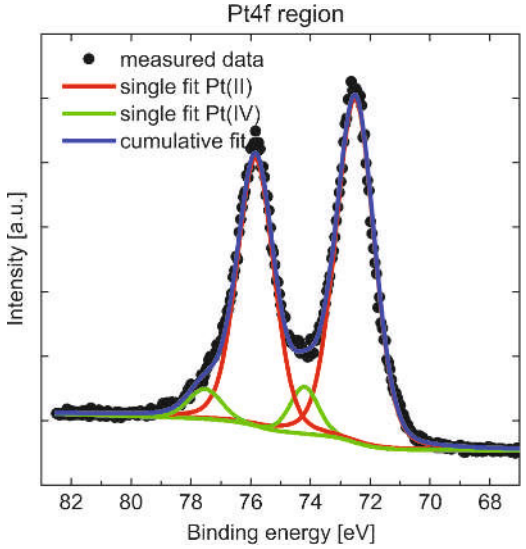

Figure 3. XPS photoelectron spectra of Pt4f core level peaks of PtNPs–GO

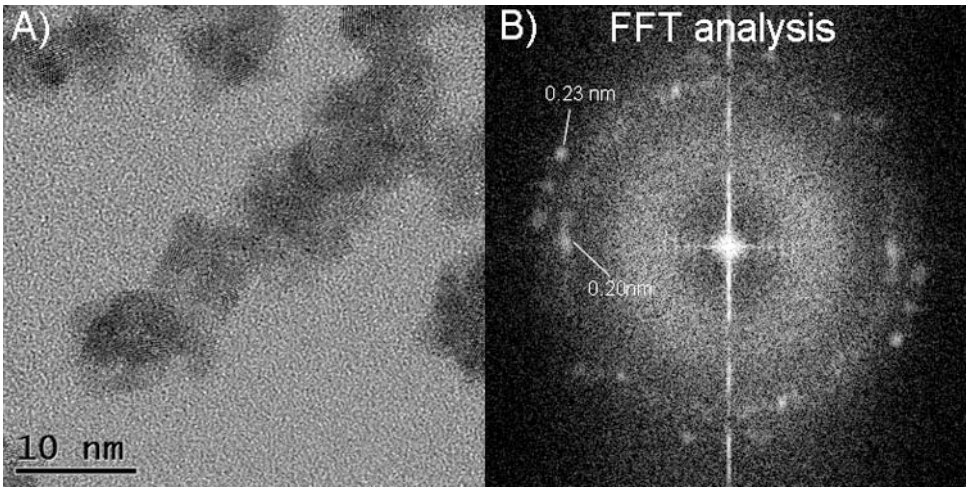

Figure 4. HRTEM and FFT analysis of PtNPs–GO

the channel. In this case, it was possible to decrease this distance about 3 times. It should be pointed out that, because of keeping the channel size, the pressure drop remained small.

Microscope images analysis of the obtained samples showed that only about 71% of graphene surface was coated by platinum nanoparticles. It is probably due to the interactions between PtNPs and graphene oxide. Van Dam and Van Bekkum [22] investigated the process of Pt adsorption on the surface of activated carbon and postulated that it is possible to form π-complexes between Pt^{2+} and oxygen-containing functional groups on the basal plane edges. It is well known that PtNPs exhibit strong surface charge [18], which keeps these nanoparticles separated. This charge is probably due to the hydroxide ions adsorbed on their surface. Therefore, incomplete coverage of graphene oxide surface is observed.

Taking into account the obtained results, mass ratio of Pt to GO was calculated and is shown in Table 1.

2.2. Influence of the Flow Rate on Nanoparticle Size and Size Distribution. The influence of the flow rate on the PtNPs size and size distribution was also investigated. During these experiments, volumetric flow ratio 1:1:1 of DMAB, graphene oxide, and chloroplatinic acid was kept constant. Figure 6 shows the results of these experiments.

It can be seen that the flow rate of reagents has a slight influence on PtNPs size. However, the size distribution depends on the flow rate of the reagents. It can be also observed that, for the flow rate of 1.5 mL/min, particles reveal the widest size distribution. Increase of the flow rate up to 9 mL/min changes particle size distribution. However, the predominant fraction still remains at the level of 2−3 nm.

It can be seen from Table 2 and Figure 7 that it is possible to decrease the synthesis time down to 5.6 without significant loss in the quality of the formed product. Probably, the further increase of the flow rate of the reagents may cause composite material deposition on the bends of the microreactor channels in effect of centrifugal forces.

The results of wavelength dispersive spectroscopy (WDS) analysis (wavelength dispersion X-ray spectroscopy) of the obtained material are shown in Figure 7. The sample of PtNPs–GO was obtained in the experiment with the flow rate of 3 mL/min, $C_{0,Pt(IV)}=2.5\times10^{-4}$ M, $C_{0,GO}=3.3\times10^{-2}$ g/L, and $C_{0,DMAB}=3.3\times10^{-3}$ M. Two outstanding peaks can be seen. The first comes from platinum and the second from copper. Also, some peaks from aluminum, oxygen, and carbon can be observed. Signal from copper can be explained as an artifact resulting from copper mesh which was used to deposit the obtained samples. Aluminum-made element was used to hold a grid during the analysis. Oxygen and carbon can be related to graphene oxide sheet, as well as to amorphous carbon which was used to coat copper grid.

2.3. UV–Vis Analysis of PtNPs–GO. The results of UV–vis analysis of the obtained colloidal suspension are shown in Figure 8. In this figure, three peaks at the wavelength 218, 229, and 259 nm, respectively, can be observed. The peak at the wavelength 229 nm can be assigned to the π–π* transition of aromatic C−C bonds [1f]. Peaks at 218 and 259 nm can be assigned to plasmon resonance of platinum nanoparticles. Gharibshahi and Saion [23] have shown that platinum nanoparticles with average size in the range from 3.4 to 5.3 nm absorb light in the UV range.

Theoretical calculations [23] for a single PtNPs of diameter 5.3 nm have shown that such nanoparticles absorb light at the wavelength 217.1 and 265.1 nm. The obtained results are in good agreement with these literature data. The slight shift of the absorption peak of PtNPs can be related to the shape of those particles. It is known that the shape has significant influence on the UV–vis spectra of colloidal gold [24], silver [25], and platinum [23] nanoparticles.

2.4. FT-IR Analysis of PtNPs at GO. The obtained material was also analyzed using FT-IR method. The results are shown in Figure 9. Green line represents the obtained material (PtNPs–GO), red line corresponds to graphene oxide, and the black one to the reductant (DMAB) used in the synthesis process. It should be pointed out that the sample was dialyzed before analysis to remove an excess of the reductant and other salts.

Significant changes in the IR spectra can be seen after deposition of PtNPs at the surface of GO. There are several strong peaks disappearing after the process of the composite material synthesis. The first one at 3460/cm, associated with O–H stretching, seems to disappear after platinum deposition. The next strong peaks at 1726 and 1625/cm are associated with C=O stretching. It can be seen that the intensity of those peaks decreases after reduction of Pt(IV) and nanoparticles deposition at the surface of GO. Moreover, after synthesis procedure, several new peaks at 1380 and 1310/cm can be observed in the final product. The first one can be attributed to C–O stretching, and the second one, to carboxylic functional groups.

Since higher concentration of PtNPs can be noted on the edges of GO (see Figure 1 and Figure 2), one may speculate that it may be related with the chemical properties of graphene oxide sheets. In general, it can be assumed that the edges of GO are mainly decorated by carboxylic acids groups with epoxyl and hydroxyl groups on the basal plane [26]. Chiu and Huang [26b] reported that the amine groups and the carboxylic acid group bind to form a strongly covalent bond. The dimethyloamina

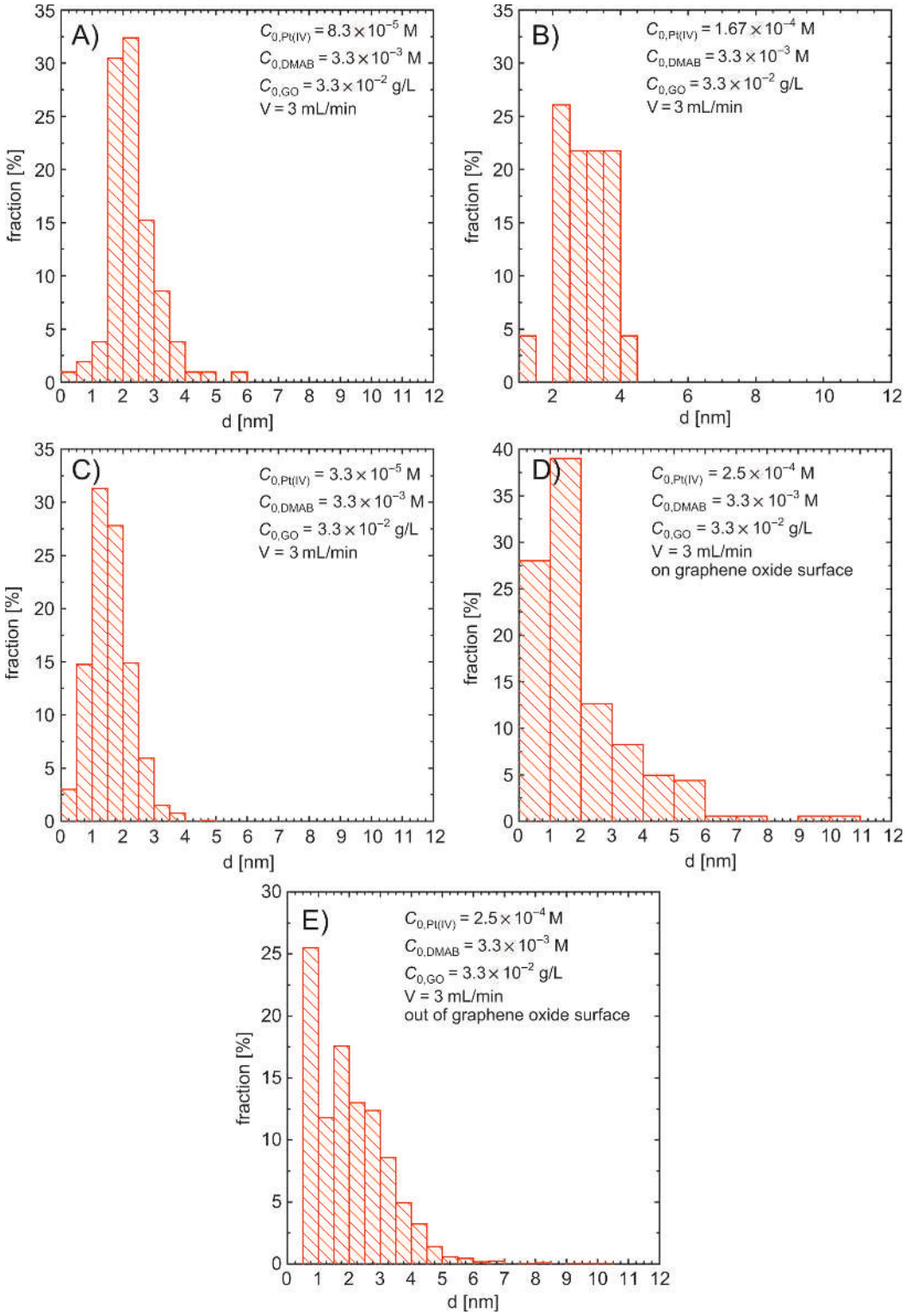

Figure 5. Particle size distribution as a function of the initial concentration of platinum(IV) ($C_{0,GO}$=3×10^{-2} g/L, $C_{0,DMAB}$=3×10^{-3} M, pH=13)

$(CH_3)_2NH$) is formed in statu nescendi during reduction of Pt(IV) to Pt and oxidation of DMAB. This compound may remain at the surface of the PtNPs, binding them to the edges of graphene oxide.

Table 1. Mass ratio of Pt to GO

Initial concentration of Pt(IV)	Amount of PtNPs in the composite (%)
8.3×10^{-5} M	17.8
1.67×10^{-4} M	35.1
3.3×10^{-4} M	52.0
2.5×10^{-4} M	61.9[a]/52

[a] Theoretical, assuming that 100% Pt is bonded to graphene oxide.

Furthermore, it can be suggested that reduction of graphene oxide (rGO) also takes place during the process. Bose et al. [27] observed the decrease of O–H functional groups concentration during the reduction of graphene oxide using glycine as the reducing agent. However, it cannot be excluded that Pt clusters preferably adsorb on O–H functional groups.

Dreyer et al. [28] has pointed out that GO is generally a poorly conductive material due to its disrupted sp^2 bonding network. The increase of conductivity can be achieved by restoring the π-network, which in turn can be obtained, e.g., by reduction of graphene oxide. After that, it can be successfully used in electro-oxidation processes.

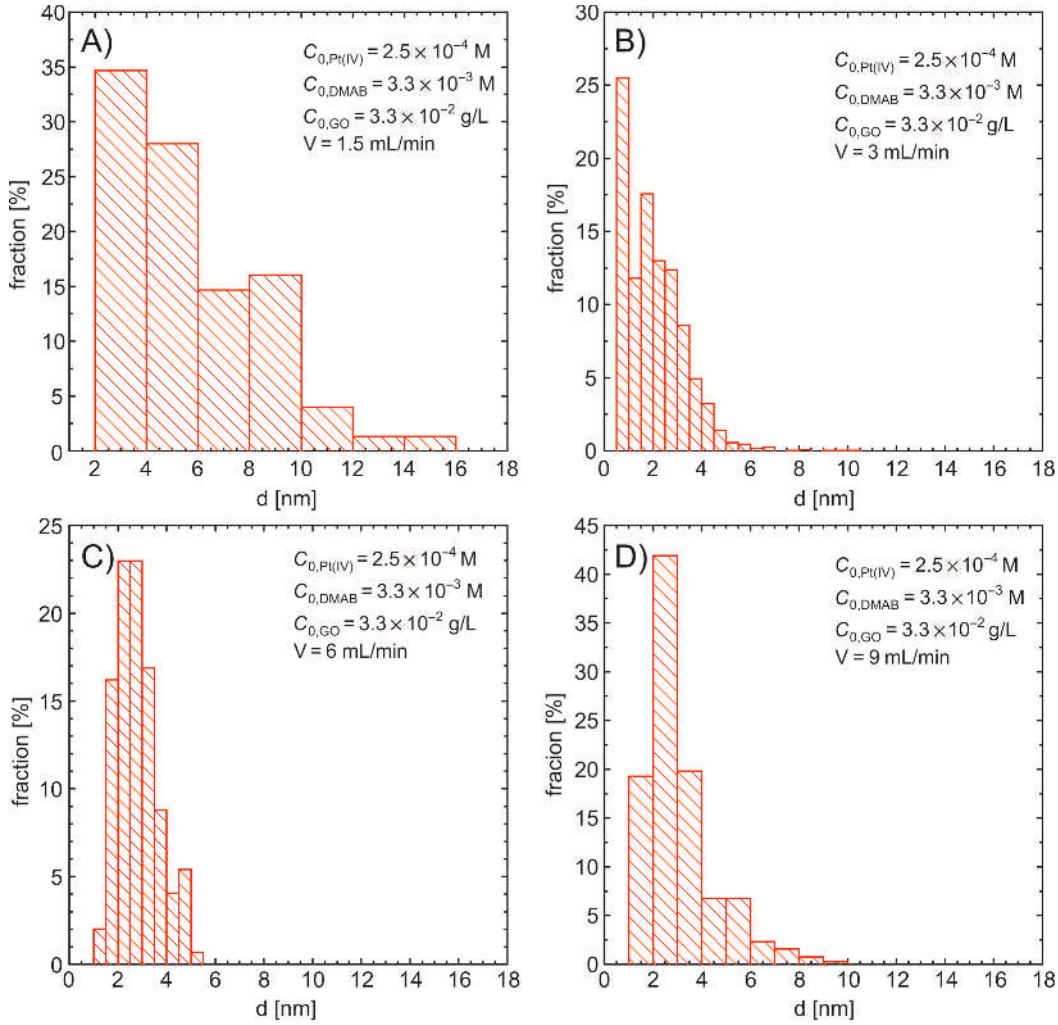

Figure 6. Particle size and size distribution as a function of the flow rate

2.5. Electro-Oxidation of Glucose onto PtNPs–rGO–GC Electrodes. Recently, a lot of attention has been paid to applications of nanoparticles towards electrocatalytic oxidation of glucose in energy conversion systems [12a, 29] or electrochemical glucose detectors [30]. A large number of electrons liberated by glucose oxidation reaction:

$$C_6H_{12}O_6 + 24OH^- \rightarrow 6CO_2 + 18H_2O + 24e \qquad (1)$$

makes it possible to generate electricity in fuel cells. In this paper, we also investigated properties of PtNPs–rGO-covered glassy carbon electrodes towards electrochemical glucose oxidation reaction.

In voltammetric tests, Ag–AgCl electrode ($E_{Ag/AgCl}{}^0$=0.210 mV, 3 M KCl at 298 K) was used. The results are presented versus reversible hydrogen electrode (RHE) (eq. (2)).

$$E_{RHE} = E_{Ag/AgCl} + 0.059 \cdot pH + E^0_{Ag/AgCl} \qquad (2)$$

The measurements were performed at the scan rate of 100 mV/s at 298 K. As a catalyst, PtNPs–rGO obtained during experiments described above was used (Figure 5D). The results of performed electrochemical tests are presented in Figure 10. All current densities correspond to electrochemically active surface (EAS), estimated using the data presented in Figure 5D. EAS values for glassy carbon (GC) electrodes covered with different volume of colloid containing PtNPs–rGO particles (10, 30, and 60 μL, respectively) were calculated with eq. (3) [5b]:

$$EAS = \sum_{i=1}^{n} \left(N_i \cdot 4 \cdot \pi \cdot R_i^2\right) \qquad (3)$$

where:

R_i — radius of i-th fraction of platinum nanoparticles,

N_i — number of particles of radius R_i, which is described by:

$$N_i = \frac{\left(C_{0,\,Pt(IV)} \cdot V \cdot M_{m,\,Pt}\right) \cdot Fr_i}{\rho_{Pt} \cdot \frac{4}{3} \cdot \pi \cdot R_i^3} \qquad (4)$$

where:

$M_{m,\,Pt}$ — molar mass of platinum (195.08 g/mol),

$C_{0,\,Pt(IV)}$ — initial concentration of platinum salt ($2.5 \cdot 10^{-4}$ M),

V — volume of colloid used in synthesis of electrode (10, 30, and 60 μL, respectively),

Table 2. Flow parameters through microreactor

Total flow rate (mL/min)	Reynold's number in micromixer section	Reynold's number in microreactor section	Linear velocity in micromixer section (m/s)	Linear velocity in microreactor section (m/s)	Resident time in the microreactor (s)
1.5	70.98	58.46	0.171	0.086	33.7
3	141.96	116.91	0.342	0.171	16.9
6	283.93	233.83	0.685	0.342	8.4
9	425.89	350.74	1.027	0.513	5.6

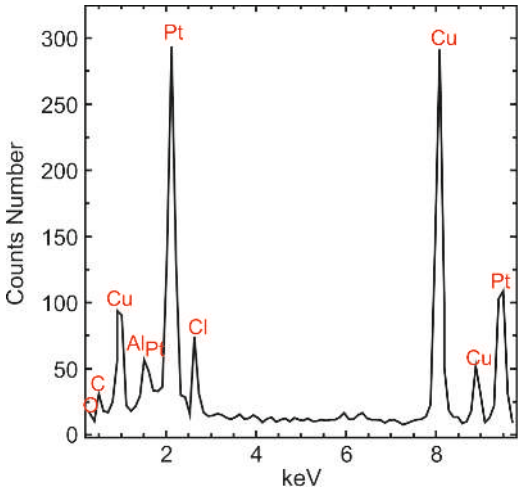

Figure 7. WDS spectrum for the obtained material

ρ_{Pt} — platinum density (21.09 g/cm^3),
Fr_i — fraction of PtNPs–rGO particles in %.

Estimated EAS values for particular colloid volumes are equal to 0.469, 1.407, and 2.345 cm^2, respectively.

Figure 10A presents linear voltammograms (LVs) registered under different conditions within the potential range from −0.25 to 0.8 V. Peaks are not present on the voltammogram registered for GC PtNPs–rGO free electrode within applied potential range. LVs registered for GC electrode covered with PtNPs–rGO catalyst indicate peak at c.a. 0.31 V vs. reference hydrogen electrode (RHE). The observed current increase is connected with glucose oxidation, resulting in production of 24 electrons per molecule according to reaction (1).

Dependence of current density vs. PtNPs–rGO colloid volume addition shows asymptotic character (see Figure 10B). It can be concluded that an increase in the density of nanoparticles deposited at GC electrode does not cause an increase of current resulting from glucose oxidation. GC electrodes covered with 60 μL of colloid were used for tests in electrolytes with glucose concentration ranging from 5 to 20 mM (Figure 10A). The current density corresponding to peak maxima as a function of glucose concentration shows linear character with R^2=0.973 (Figure 10B). It can be concluded that, within applied glucose concentrations range, investigated PtNPs–rGO–GC can be used for qualitative as well as quantitative investigations. The presented results show that PtNPs–rGO–GC composite material

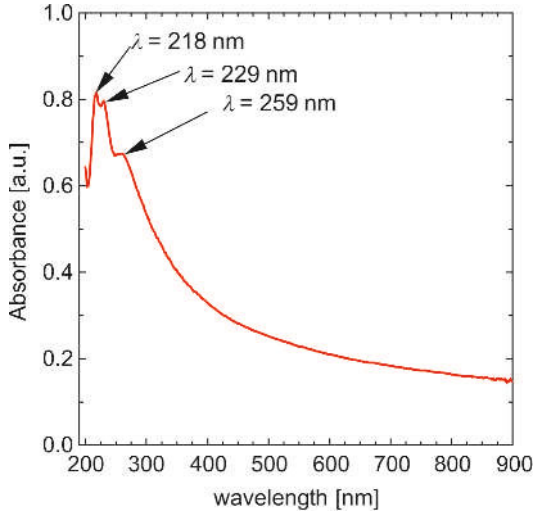

Figure 8. UV–vis spectra of colloidal suspension of PtNPs at graphene oxide sheets

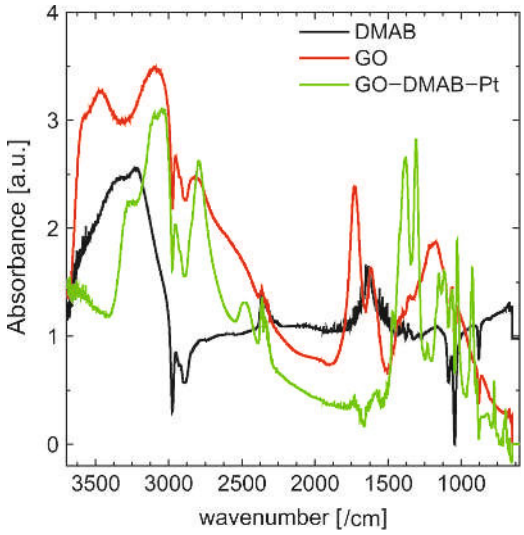

Figure 9. FT-IR analysis of the obtained material

exhibits promising properties towards the application in glucose sensing systems.

3. Conclusion

It was demonstrated that a single step platinum nanoparticles synthesis and deposition on graphene oxide sheets can be achieved using a microflow reactor. The flow rate has insignificant influence on the average particle size. However, it was shown that, for the lowest flow rate (1.5 mL/min) and for the highest flow rate (9 mL/min), a higher dispersion of particles was observed. Increasing the flow rate up to 9 mL/min results in shorter synthesis time without loss in the quality of the obtained final product. This in turn may pay off in decreasing the production costs.

The influence of PtNP's size on their catalytic properties is still a matter of investigations because of the difficulties in controlling particle size without changes of other parameters, such as lattice parameter and surface chemical properties [32]. It is suggested that either subnanometric particles cannot act as a catalyst or their catalytic properties are lower when oxidized molecule is larger than the catalyst. It is known that the diameter of the glucose molecule is equal to 1.5 nm [33]. Our experiments showed that PtNPs–rGO did not catalyze methanol oxidation whose molecule size is smaller than that of glucose (kinetic diameter of methanol is equal to 0.38–0.41 nm) [34]. This fact in turn clearly suggests that not only the size but also surface characteristics of PtNPs particles, such as surface chemical properties, have a significant influence on the catalytic properties. Xie L. et al. [35] investigated the process of platinum cluster growth on carbon surface. They have shown that particles with size less than 1 nm show only the presence of platinum in the form of PtO_xH_y species. For nanoparticles with size in the range of 2.5–3 nm, external layer consists of atoms at 2^+ oxidation state. The core of the nanoparticle is made of metallic platinum [36]. The XPS analysis demonstrated that about 91% of Pt in the obtained material exists in 2+ oxidation state and about 9% in 4+. This result supports our previous assumption that no catalytic properties to oxidation of methanol by the obtained composite can be related with the surface chemistry of Pt–GO particles. Taking into account that the depth of XPS analysis depends on the beam energy, it cannot be excluded that the obtained material has core–shell-like structure, where the core consists of metallic Pt and the shell of PtO_xH_y.

The catalytic properties of the synthesized materials were investigated in two independent systems. The first one has been described in detail in the present paper. The second consisted in

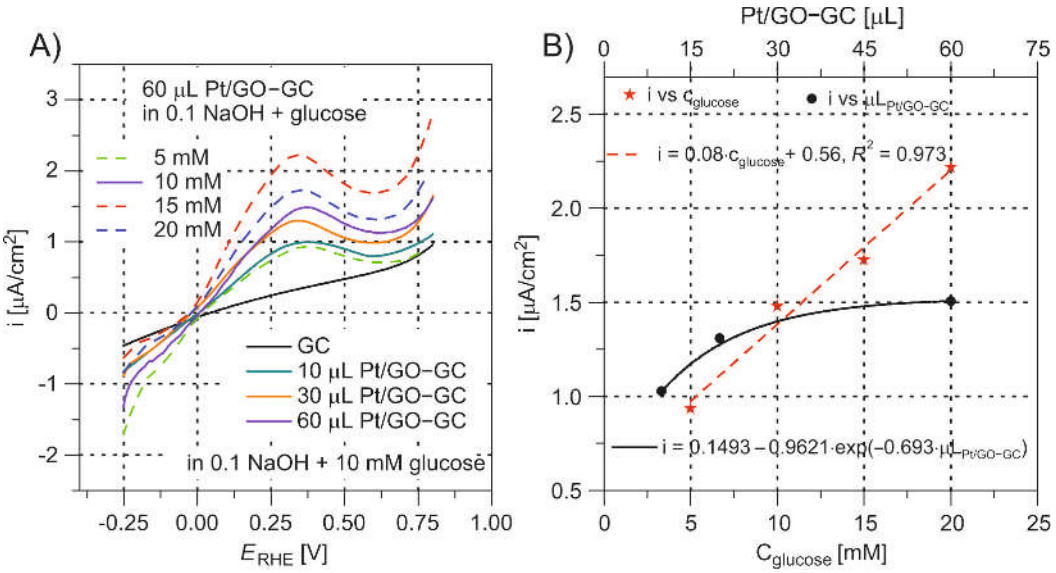

Figure 10. Linear voltammograms registered for glucose electrooxidation process on electrodes prepared by deposition of different Pt–GO colloid volume (0.1 M NaOH, 10 mM glucose) (A) and in electrolytes of different glucose concentration (0.1 M NaOH, 60 µL of PtNPs–rGO–GC) (B), pH=13

the electro-oxidation of methanol in acidic media (0.1 M of methanol in 0.1 M $HClO_4$) and revealed no catalytic effect. The obtained materials show catalytic properties during electro-oxidation of glucose in alkaline media (pH=13). The registered current densities in the range of applied concentrations of glucose confirm that the tested materials exhibit catalytic properties comparable to those presented in the literature [31]. Wu et al. [30] tested non-enzymatic electrochemical glucose sensor based on Pt in the form of nanoflowers deposited on the surface of graphene oxide. They demonstrated that, within the investigated glucose concentration range (from 10.3 to 20.3 mM), their electrodes exhibit a sensitivity of 0.6 µAm/M/cm^2. In our case, the sensitivity is c.a. 7.5 times lower. The difference is probably due to different methodology of EAS measurements. In our case, it was assumed that all nanoparticles participate in glucose oxidation. However, about 65% of nanoparticles have the size smaller than the size of glucose molecule.

4. Experimental

In all experiments, deionized water was used (Hydrolab HLP-30) in impurity concentrations: Na^+, SO_4^{2-}, Cl^-, Br^-, NO_2^-, NO_3^-, PO_4^{3-} <0.5 ppb, Fe, Zn, Cu, Cr, Mn <0.1 ppb, and conductivity <0.07 S/cm.

As a platinum nanoparticles precursor, hexachloroplatinate acid (H_2PtCl_6) was used. Hexachloroplatinate acid was obtained by dissolution of metallic platinum (Mennica Polska S.A., 99.99%) in aqua regia. The obtained solution was purified by distillation, to remove excess of nitric acid. As a reducing agent, dimethylamino borane complex (DMAB) was applied without further purification (>96%, Fluka). It is well known that DMAB is unstable in aqueous solutions; however, in alkaline environment, DMAB can be stored for a long period of time. To control the pH of the solution, sodium hydroxide was used (POCH S.A.).

The specimens for microstructure observations were prepared by placing a drop of colloidal suspension containing graphene oxide or platinum-coated graphene sheets in an aqueous suspension (10 min after preparation) on to a copper grid covered by a 20−30 nm carbon film, and then dried at room temperature. The analyses were performed by using scanning electron microscope (SEM — Hitachi SU-70) as well as high-resolution scanning transmission electron microscope (HRSTEM — Hitachi HD-2700).

Particle size and size distribution were determined using ImageJ application (ver. 1.48b). During this analysis, several assumptions were made, e.g., circularity of particles was set up within the range from 0.5 to 1. Only particles in the size range from 0.05 nm to 50 nm were taken into account. Threshold of PtNPs detection was set up manually. Agglomerates were excluded from calculations as well as single pixels.

For the synthesis of composite material, commercially available graphene oxide (GO), supplied by Graphene Supermarket®, in the form of aqueous colloidal suspensions (intense brown color) which contained 5 g/L of GO was used. To obtain the required concentration of GO, dilution in 0.1 M of NaOH was applied. It is well known that GO exhibits hydrophilic nature, and thanks to that, stable aqueous suspensions may form [3a]. The size of graphene oxide flakes varies from 0.5 to 0.7 µm (see Figure 11). Over 60% of the dispersed graphene oxide has the thickness of one atomic layer.

To prevent piston pump damage, the sample loop for GO suspension of 10 mL volume was used.

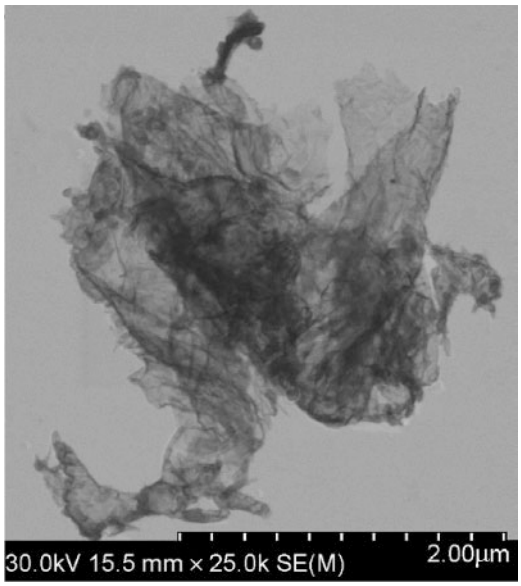

Figure 11. SEM image of the graphene oxide sheet

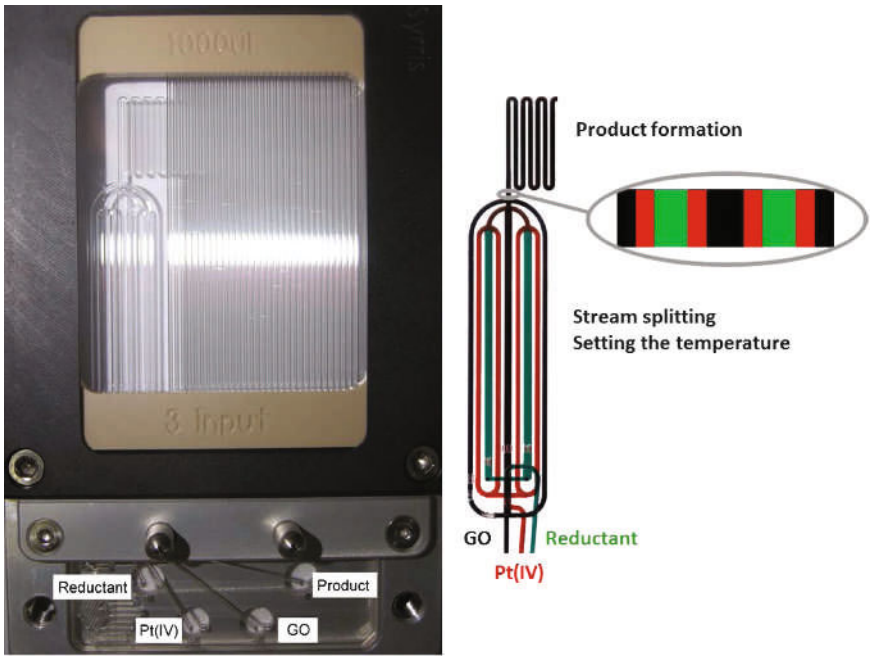

Figure 12. View of the 3-input microflow reactor

All experiments related to PtNPs synthesis and their deposition on GO have been carried out in 3-input microflow reactor (Syrris, England) shown in Figure 12. This chip is made of glass, with the total volume of 1 mL. Knowing the flow rate, as well as the total volume of the reactor, the resident time of reagent in the chip can be calculated using the following relation:

$$t = \frac{V_r}{F_r} \tag{5}$$

where
t — resident time of reagent in the chip (min),
V_r — total volume of the reactor (mL),
F_r — flow rate of reagents (mL/min).

Reagent flow rates were changed within the range from 0.5 to 9 mL/min. This, in turn, effects significant changes in resident time of reagent in the microflow reactor from 6.7 up to 120 s. As it can be easily calculated, application of single reactor results to production of above 0.5 L of the final product per hour. Applied glass microreactor consists of two main parts. In the first one, the reagents are divided into several substreaming: in the case of GO, 3 streams (black color in Figure 12); in the case of Pt(IV), 4 streams (red color in Figure 12); and in the case of DMAB, 2 streams (green color in Figure 12). Thanks to that, thermal equilibrium can be reached faster. Then, those streams are sequentially combined to one. In the first step, reductant and Pt(IV) ions are mixed in static mixer and then are statically mixed with GO. Thanks to solution dividing and again conation, the average diffusion path was decreased significantly. It should be pointed out that, in the case of graphene oxide (diameter of 0.5 to 0.7 μm), the diffusion rate is low.

Detailed information about channel geometry design as well as demotion of the channels can be found in the supporting information (Figure S1 and Table S1, respectively).

Electrochemical properties of PtNPs–GO were determined using aqueous (0.1 M) solution of glucose (POCH, P.A.) and (0.1 M) solution of sodium hydroxide (POCH, S.A). The main aim of electrochemical studies was to investigate the influence of the density of PtNPs on GO on kinetics of glucose electro-oxidation reaction. Electrochemical studies of electro-oxidation of glucose were performed in conventional three-electrode electrochemical cell with the use of AUTOLB PGSTAT30 potentiostat/galvanostat. The working electrode (WE) was GC electrode covered with different volume of Pt–GO colloid containing Nafion® on polished GC electrode of 0.196 cm^2 surface area. Before colloid deposition, GC electrodes were polished with the use of 0.1 μm Al_2O_3 suspension. The Pt sheet as a counter electrode and Ag–AgCl (3 M KCl) as a reference electrode were applied.

Before electrochemical tests, aqueous suspension of PtNPs–GO was dialyzed for 7 days to remove an excess of reductant and other salts that remained in the solution after synthesis using cellophane membrane. Moreover, PtNPs–GO material purified by dialysis was used in FT-IR and XPS analysis. Before those analyses, water was evaporated. For those purposes, Nicolet 380 FT-IR spectrometer (Thermo Scientific) and PHI 5000 VersaProbe II (ULVAC-PHI, Chigasaki, Japan) system using a microfocused (100 μm, 25 W) Al Kα X-ray beam with a photoelectron take-off angle of 45° were used respectively. In the case of XPS analysis, a dual-beam charge neutralizer was used to compensate the charge-up effect. The operating pressure in the analytical chamber was less than 2×10^{-9} mbar. High-resolution spectra were collected with analyzer pass energy of 23.50 eV. All XPS peaks were charge referenced to the neutral (C–C) carbon C1s peak at 284.8 eV. Spectrum background was subtracted using the Shirley method.

Acknowledgment. This work was supported by the European Grant no. POIG.01.01.02.-00-015/09-00 and AGH University of Science and Technology (contract no. 11.11.180.373.2012).

The authors thank A. Podborska (AGH University of Science and Technology, Department of Physical Chemistry and Metallurgy of Non-Ferrous Metals) for her help during FT-IR analysis as well as M. Marzec (AGH University of Science and Technology, Academic Centre for Materials and Nanotechnology) for his help during XPS analysis.

K. Mech gratefully acknowledges the financial support of the Foundation for Polish Science within the Start scholarship (072.2014).

Also, we are grateful to A. Stratton (MEGANTECH (www.megantech.pl)) for his help and delivery of the microflow system.

Supporting Information

Electronic Supplementary Material (ESM) is available in the online version at doi: 10.1556/JFC-D-14-00032.

Reference

1. (a) Stankovich, S.; Pine, R. D.; Nguyen, S. T.; Ruoff, R. S. *Carbon* **2006,** *44*, 3342–3347; (b) Stankovich, S.; Dikin, D. A.; Piner, R. D.; Kohlhaas, K. A.; Kleinhammes, A.; Jia, Y.; Wu, Y.; Nguyen, S. T.; Ruoff, R. S. *Carbon* **2007,** *45*, 1558–1565; (c) Seyller, T.; Bostwick, A.; Emtsev, K. V.; Horn, K.; Ley, L.; McChesney, J. L.; Ohta, T.; Riley, J. D.; Rotenberg, E.; Speck, F. *Phys. Status Solidi B* **2008,** *245*, 1436–1446; (d) Wang, G.; Wang, B.; Park, J.; Yang, J.; Shen, X.; Yao, J. *Carbon* **2009,** *47*, 68–72; (e) Zhu, C.; Guo, S.; Fang, Y.; Dong, S. *ACS Nano* **2010,** *4*, 2429–2437; (f) Zhang, Y.; Ma, H.-L.; Zhang, Q.; Peng, J.; Li, J.; Zhai, M.; Yu, Z.-Z. *J. Mater. Chem.* **2012,** *22*, 13064–13069.

2. (a) Katsnelson, M. I. *Graphene: Carbon in Two Dimensions*; Cambridge University Press, 2012; (b) Choi, W.; Lee, J. *Graphene: Synthesis and Applications*; CRC Press, 2012; (c) Rao, C. N. R.; Sood, A. K. *Graphene: Synthesis, Properties, and Phenomena*; Wiley, 2013.

3. (a) Pei, S.; Cheng, H.-M. *Carbon* **2012,** *50*, 3210–3228; (b) Pham, V. H.; Pham, H. D.; Dang, T. T.; Hur, S. H.; Kim, E. J.; Kong, B. S.; Kim, S.; Chung, J. S. *J. Mater. Chem* **2012,** *22*, 10530–10536.

4. Leenaerts, O.; Partoens, B.; Peeters, F. M. *Phys. Rev. B: Condens. Matter Mater. Phys.* **2009,** *79*.

5. (a) Muszynski, R.; Seger, B.; Kamat, P. V. *J. Phys. Chem* **2008,** *112*, 5263–5266; (b) Wojnicki, M.; Luty-Błocho, M.; Dobosz, I.; Grzonka, J.; Pacławski, K.; Kurzydłowski, K.; Fitzner, K. *Mater. Sci. Appl.* **2013,** *4*, 162–169; (c) Wojnicki, M.; Luty-Błocho, M.; Grzonka, J.; Pacławski, K.; Kurzydłowski, K. J.; Fitzner, K. *Chem. Eng. J.* **2013,** *225*, 597–606; (d) Xue, Y.; Zhao, H.; Wu, Z.; Li, X.; He, Y.; Yuan, Z. *Biosens. Bioelectron.* **2011,** *29*, 102–108.

6. Tien, H.-W.; Huang, Y.-L.; Yang, S.-Y.; Wang, J.-Y.; Ma, C.-C. M. *Carbon* **2011,** *49*, 1550–1560.

7. (a) Ghosh, A.; Basu, S.; Verma, A. *Fuel Cells* **2013,** *13*, 355–363; (b) Lu, J.; Do, I.; Drzal, L. T.; Worden, R. M.; Lee, I. *ACS Nano* **2008,** *2*, 1825–1832.

8. Shahbazali, E.; Hessel, V.; Noël, T.; Wang, Q. *Nanotechnol. Rev.* **2014,** *3*, 65–86.

9. Watson, D. J.; Attard, G. A. *Electrochim. Acta* **2001,** *46*, 3157–3161.

10. (a) Jin, C.; Chen, Z. *Synth. Met.* **2007,** *157*, 592–596; (b) Park, I.-S.; Lee, K.-S.; Jung, D.-S.; Park, H.-Y.; Sung, Y.-E. *Electrochim. Acta* **2007,** *52*, 5599–5605.

11. Basu, D.; Basu, S. *Electrochim. Acta* **2010,** *55*, 5775–5779.

12. (a) Tang, Y.; Zhang, L.; Wang, Y.; Zhou, Y.; Gao, Y.; Liu, C.; Xing, W.; Lu, T. *J. Power Sources* **2006,** *162*, 124–131; (b) Tang, Y. W.; Li, G.; Liu, C. P.; Xing, W.; Lu, T. H. *Chin. Chem. Lett.* **2004,** *15*, 875–878; (c) Li, Y.; Gao, W.; Ci, L.; Wang, C.; Ajayan, P. M. *Carbon* **2010,** *48*, 1124–1130.

13. Chen, S.; Xu, R.; Huang, H.; Yi, F.; Zhou, X.; Zeng, H. *J. Mater. Sci.* **2007,** *42*, 9572–9581.

14. (a) Wojnicki, M.; Pacławski, K.; Socha, R. P.; Fitnzer, K. *Trans. Nonferrous Met. Soc. China* **2013,** *23*, 1147–1156; (b) Adora, S.; Soldo-Olivier, Y.; Faure, R.; Durand, R. *J. Phys. Chem. B* **2001,** *105*, 10489–10495; (c) Gomesa, H. T.; Serpb, P.; Kalckb, P.; Figueiredoa, J. L.; Fariaa, J. L. *Top. Catal.* **2005,** *33*, 59–68.

15. (a) Tanga, Z.; Poh, C. K.; Lee, K. K.; Tian, Z.; Chua, D. H. C.; Lin, J. *J. Power Sources* **2010,** *195*, 155–159; (b) Mason, C. W.; Kannan, A. M. *ISRN Nanotechnol.* **2011**, *2011*, article ID 708045, 6 pages, http://dx.doi.org/10.5402/2011/708045.

16. Hessel, V.; Löwe, H. *Chem. Eng. J.* **2003,** *26*, 391–408.

17. (a) Luty-Błocho, M.; Fitzner, K.; Hessel, V.; Löb, P.; Maskos, M.; Metzke, D.; Pacławski, K.; Wojnicki, M. *Chem. Eng. J.* **2011,** *171*, 279–290; (b) Luty-Błocho, M.; Wojnicki, M.; Grzonka, J.; Kurzydłowski, K. J. *Arch. Metall. Mater.* **2014,** *59*, 509; (c) Sebastián, V.; Lee, S.-K.; Zhou, C.; Kraus, M. F.; Fujimoto, J. G.; Jensen, K. F. *Chem. Commun.* **2012,** *48*, 6654–6656; (d) Torigoe, K.; Watanabe, Y.; Endo, T.; Sakai, K.; Sakai, H.; Abe, M. *J. Nanopart. Res.* **2010,** *12*, 951–960; (e) Günthera, P. M.; Großa, G. A.; Wagnera, J.; Jahnb, F.; Köhlera, J. M. *Chem. Eng. J.* **2008,** *1355*, S126–S130.

18. Luty-Błocho, M.; Wojnicki, M.; Pacławski, K.; Fitzner, K. *Chem. Eng. J.* **2013,** *226*, 46–51.

19. Porsgaard, S.; Merte, L.; Ono, L.; Behafarid, F.; Matos, J.; Helveg, S.; Salmeron, M.; Cuenya, B.; Besenbacher, F. *ACS Nano* **2012,** *6*, 10743–10749.

20. Arico, A.; Shukla, A.; Kim, H.; Park, S.; Min, M.; Antonucci, V. *Appl. Surf. Sci.* **2001,** *172*, 33–40.

21. (a) Saidani, F.; Rochefort, D.; Mohamedi, M. *Laser Chem.* **2010,** *2010*; (b) Wagner, C. D.; Muilenberg, G. E. *Handbook of X-ray Photoelectron Spectroscopy: A Reference Book of Standard Data for Use in X-ray Photoelectron Spectroscopy*; Physical Electronics Division, Perkin-Elmer Corp., 1979.

22. Van Dam, H. E.; Van Bekkum, H. *J. Catal.* **1991,** *131*, 335–349.

23. Gharibshahi, E.; Saion, E. *Int. J. Mol. Sci.* **2012,** *13*, 14723–14741.

24. (a) Jain, P. K.; Lee, K. S.; El-Sayed, I. H.; El-Sayed, M. A. *J. Phys. Chem. B* **2006,** *110*, 7238–7248; (b) Zande, B. M. I. v. d.; Böhmer, M. R.; Fokkink, L. G. J.; Schönenberger, C. *Langmuir* **2000,** *16*, 451–458.

25. Ledwith, D. M.; Whelan, A. M.; Kelly, J. M. *J. Mater. Chem.* **2007,** *17*, 2459–2464.

26. (a) Wang, X.; Bai, H.; Shi, G. *JACS* **2011,** *133*, 6338–6342; (b) Chiu, N.-F.; Huang, T.-Y. *Sens. Actuators, B* **2014,** *197*, 35–42; (c) Hu, Y.; Li, F.; Bai, X.; Li, D.; Hua, S.; Wang, K.; Niu, L. *Chem. Commun.* **2011,** *47*, 1743–1745.

27. Bose, S.; Kuila, T.; Mishra, A. K.; Kim, N. H.; Lee, J. H. *J. Mater. Chem.* **2012,** *22*, 9696–9703.

28. Dreyer, D. R.; Park, S.; Bielawski, C. W.; Ruoff, R. S. *Chem. Soc. Rev.* **2010,** *39*, 228–240.

29. Ferreira, P. J.; O', G. J. l.; Shao-Horn, Y.; Morgan, D.; Makharia, R.; Kocha, S.; Gasteigerc, H. A. *J. Electrochem. Soc.* **2005,** *152*, A2256–A2271.

30. Wu, G.-h.; Song, X.-h.; Wu, Y.-f.; Chen, X.-m.; Luo, F.; Chen, X. *Talanta* **2013,** *105*, 379–385.

31. Zhu, Z.; Garcia-Gancedo, L.; Flewitt, A. J.; Xie, H.; Moussy, F.; Milne, W. I. *Sensors* **2012,** *12*, 5996–6022.

32. (a) Godoi, D. R. M.; Perez, J.; Mercedes Villullas, H. *J. Electrochem. Soc.* **2007,** *154*, B474-B479; (b) Srinivas, D.; Ratnasamy, P. In *Nanotechnology in Catalysis*; Zhou, B., Han, S., Raja, R., Somorjai, G., Eds.; Springer: New York, 2007; pp. 183–220.

33. Minoli, D. *Nanotechnology Applications to Telecommunications and Networking*; Wiley, 2005.

34. Ten Elshof, J. E.; Abadal, C. R.; Sekulić, J.; Chowdhury, S. R.; Blank, D. H. A. *Microporous Mesoporous Mater.* **2003,** *65*, 197–208.

35. Xie, L.; Brault, P.; Coutanceau, C.; Bauchire, J.-M.; Caillard, A.; Baranton, S.; Berndt, J.; Neyts, E. C. *Appl. Catal., B* **2015,** *162*, 21–26.

36. Sellin, R.; Clacens, J.-M.; Coutanceau, C. *Carbon* **2010,** *48*, 2244–2254.